Spindle function in *Xenopus* oocytes involves possible nanodomain calcium signaling

Ruizhen Li[a], Julie Leblanc[a,b], Kevin He[a], and X. Johné Liu[a,b,c,*]
[a]Ottawa Hospital Research Institute, Ottawa Hospital-General Campus, Ottawa, ON K1H 8L6, Canada; [b]Department of Biochemistry, Microbiology and Immunology and [c]Department of Obstetrics and Gynaecology, University of Ottawa, Ottawa, ON K1N 6N5, Canada

ABSTRACT **Intracellular calcium transients are a universal phenomenon at fertilization and are required for egg activation, but the exact role of Ca^{2+} in second-polar-body emission remains unknown. On the other hand, similar calcium transients have not been demonstrated during oocyte maturation, and yet, manipulating intracellular calcium levels interferes with first-polar-body emission in mice and frogs. To determine the precise role of calcium signaling in polar body formation, we used live-cell imaging coupled with temporally precise intracellular calcium buffering. We found that BAPTA-based calcium chelators cause immediate depolymerization of spindle microtubules in meiosis I and meiosis II. Surprisingly, EGTA at similar or higher intracellular concentrations had no effect on spindle function or polar body emission. Using two calcium probes containing permutated GFP and the calcium sensor calmodulin (Lck-GCaMP3 and GCaMP3), we demonstrated enrichment of the probes at the spindle but failed to detect calcium increase during oocyte maturation at the spindle or elsewhere. Finally, endogenous calmodulin was found to colocalize with spindle microtubules throughout all stages of meiosis. Our results—most important, the different sensitivities of the spindle to BAPTA and EGTA—suggest that meiotic spindle function in frog oocytes requires highly localized, or nanodomain, calcium signaling.**

Monitoring Editor
William Bement
University of Wisconsin

Received: May 31, 2016
Revised: Aug 24, 2016
Accepted: Aug 25, 2016

INTRODUCTION

Intracellular calcium release triggered by fertilization is a dominant biochemical event responsible for egg activation, leading to completion of meiosis and subsequent embryonic development (Whitaker, 2006; Miyazaki, 2007). In mammalian eggs, which arrest at metaphase II, fertilization-induced calcium signaling is manifested in a series of calcium waves across the whole egg lasting several hours and overlapping with sister chromatid segregation (anaphase II) and cytokinesis to emit the second polar body (Ozil, 1998). In frog eggs, which also arrest at metaphase II, only a single calcium wave is evident, which originates at the sperm entry site and travels rapidly through the cortical region to reach the antipode within 10 min (Busa and Nuccitelli, 1985; Fontanilla and Nuccitelli, 1998). A key role of calcium signaling at fertilization appears to be the activation of calcium/calmodulin-dependent protein kinase II (CMKII) (Johnson *et al.*, 1998), leading to the activation of anaphase-promoting complex (APC/C) and destruction of cyclin B and securin, thus initiating anaphase II and emission of the second polar body (Lorca *et al.*, 1993; Madgwick *et al.*, 2005). The repetitive calcium transients in mammalian eggs, in addition to their role in anaphase II initiation, are believed to be required for metabolic egg activation in preparation for embryonic development (Whitaker, 2006). However, a more recent mouse study suggested that "calcium insulation," in which both calcium efflux and calcium influx are blocked but intracellular calcium transients are unperturbed, blocks second-polar-body emission but allows anaphase II and many other egg activation events to proceed normally (Miao *et al.*, 2012). It was suggested that these eggs fail to rotate the metaphase II spindle and hence fail cytokinesis (Miao *et al.*, 2012).

Oocyte maturation, on the other hand, is triggered by species-specific intraovarian hormonal signals. Although calcium waves

This article was published online ahead of print in MBoC in Press (http://www.molbiolcell.org/cgi/doi/10.1091/mbc.E16-05-0338) on August 31, 2016.

*Address correspondence to: X. Johné Liu (jliu@ohri.ca).

Abbreviations used: APC/C, anaphase-promoting complex; BAPTA, 1,2-bis(*o*-aminophenoxy)ethane-*N*,*N*,*N*′,*N*′-tetraacetic acid; CMKII, calmodulin-dependent protein kinase II; DAPI, 4′, 6′-diamidino-2-phenylindole; DB-BAPTA, dibromo-BAPTA; EGTA, ethylene glycol tetraacetic acid; ER, endoplasmic reticulum; GFP, green fluorescent protein; GVBD, germinal vesicle breakdown; MTOC, microtubule-organizing center; OCM, oocyte culturing medium; PB, polar body; RFP, red fluorescent protein; UV, ultraviolet.

have been detected in mouse oocytes undergoing spontaneous maturation in vitro before germinal vesicle breakdown (GVBD; Carroll and Swann, 1992), they do not appear to be required for GVBD in mice (Tombes *et al.*, 1992). On the other hand, many studies have reported the lack of global calcium transients during first-polar-body emission in mice (Tombes *et al.*, 1992; Hyslop *et al.*, 2004; Marangos and Carroll, 2004), and yet depleting external calcium and, to a lesser degree, chelating intracellular calcium with 1,2-bis(2-aminophenoxy)ethane-*N*,*N*,*N*′,*N*′-tetraacetic acid (BAPTA) inhibit first-polar-body emission (Tombes *et al.*, 1992). Moreover, in frog oocytes, removal of external calcium, depletion of intracellular calcium stores by thapsigargin, or injection of BAPTA inhibited first-polar-body emission (Sun and Machaca, 2004).

This paradox—clear inhibition of first-polar-body emission by disruption of calcium signaling and yet no evidence of global calcium transients—could be explained if polar body emission requires localized calcium transients. In this study, we combined live-cell imaging with timely application of calcium chelators to examine the immediate effect of intracellular calcium buffering on polar body emission. We also used two calcium probes, Lck-GCaMP3 and GCaMP3, membrane and nonmembrane versions of the same permutated green fluorescent protein (GFP)–calmodulin–M13 core (Tian *et al.*, 2009; Shigetomi *et al.*, 2010a), respectively, to determine possible local calcium transients during polar body emission.

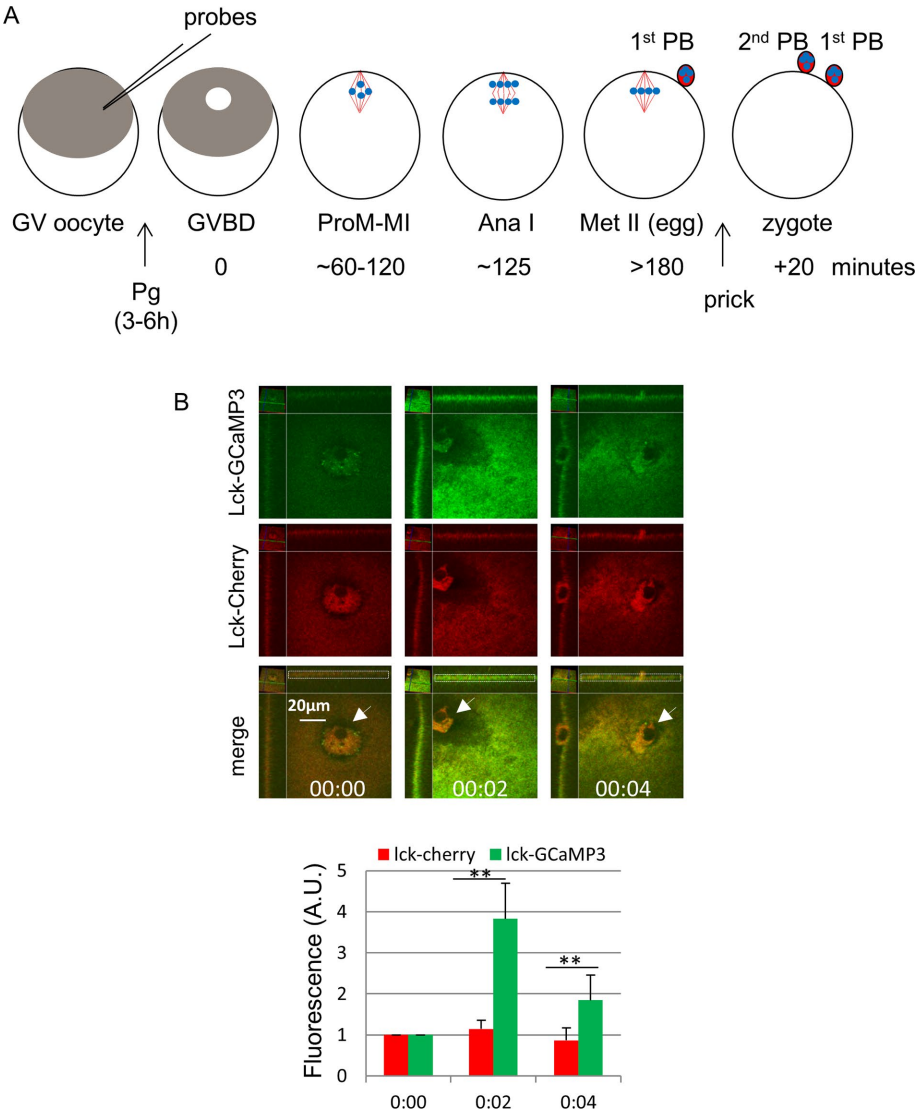

FIGURE 1: Lck-GCaMP3–detected global calcium transients at egg activation. (A) Time line of experimental approach. All fluorescent probes (mostly mRNAs) were injected at GV stage. Frog oocytes (1.4 mm in diameter) exhibit a dark-pigmented animal hemisphere and a light vegetal hemisphere. GVBD is manifested with depigmentation at the center of the animal hemisphere ("maturation spot"), where all meiosis steps occur (and are imaged). Ana I, anaphase I; MI, metaphase I; MII, metaphase II; PB, polar body; Pg, progesterone; ProM, prometaphase; red lines, spindle microtubules; blue dots, chromosomes. (B) An MII oocyte injected with mRNAs for Lck-GCaMP3 and Lck-mCherry was imaged before (00:00) and at the indicated time after prick activation. The relative position shift, as marked by the first polar body (arrows), was due to the cortical contraction characteristic of egg activation. The graph shows relative fluorescence of the cortical region surrounding the first polar body (white dotted box), with values at 00:00 set as 1 (three oocytes, two experiments). $^{**}p < 0.001$.

RESULTS

Lck-GCaMP3 and GCaMP3 failed to detect calcium transients during oocyte maturation

To detect possible calcium transients during polar body emission, we used Lck-GCaMP3, a membrane-bound calcium probe with EC_{50} = 153 nM for calcium (Shigetomi *et al.*, 2010a). The core of this probe (GCaMP) is a permutated GFP containing the Ca^{2+} sensor calmodulin at one end and M13 peptide of myosin light chain kinase at the other. Calcium binding triggers calmodulin–M13 binding, resulting in a circularized and fluorescent GFP (Nakai *et al.*, 2001). As a control, we generated Lck-Cherry, a red fluorescence version of GFP (von Dassow *et al.*, 2009). The Lck sequence contains sites of protein myristylation and palmitoylation (Yurchak *et al.*, 1996), anchoring the fusion proteins to cellular membranes. We first determined the response of these probes in *Xenopus* eggs to the well-characterized calcium wave triggered by fertilization. We injected oocytes with mRNAs coding for Lck-GCaMP3 and Lck-Cherry and incubated them with progesterone to complete meiosis I (Figure 1A). Mature (metaphase II) eggs were imaged to determine the basal fluorescence signals of the two probes, focusing on the animal pole including the first polar body (Figure 1B, 00:00, arrow). The eggs were then pricked (mimicking fertilization; Leblanc *et al.*, 2011), followed immediately by time-lapse confocal imaging. Robust Lck-GCaMP3 (enhanced GFP [eGFP]) signal was observed at the animal pole cortex 2 min after pricking (Figure 1B, 00:02, top, and graph), consistent with the traveling speed of the calcium wave (Miller *et al.*, 1993) initiated at the site of pricking (one-fourth of pole-to-pole distance). The signal subsided 2 min later (Figure 1B, 00:04, top, and graph), indicating the passing of the calcium wave peak. In contrast, cortical Lck-Cherry signal was unchanged throughout (Figure 1B, middle, and graph). These results clearly indicated that

Lck-GCaMP3 functioned as a calcium sensor in frog oocytes, responding robustly to the calcium increase at egg activation.

We next carried out live-cell imaging during oocyte maturation, focusing on first-polar-body emission. Oocytes were injected with mRNAs for red fluorescent protein (RFP)–H2B and Lck-GCaMP3, incubated with progesterone, and monitored for GVBD. Lck-GCaMP3 exhibited a slight plasma membrane signal in GV oocytes (unpublished data), and this remained unchanged up to the time of metaphase-to-anaphase transition (Figure 2A, 00:00). Soon after anaphase initiation (Figure 2A, 00:04), the cortical signal appeared to increase around the position of the contractile ring (Figure 2A, 00:06; Zhang *et al.*, 2008) and continued to increase as the membrane constricted to sever the polar body chromosomes (Figure 2A, 00:08 and 00:10). This signal persisted for hours while the egg was arrested at metaphase II (unpublished data).

Oocytes injected with Lck-Cherry together with eGFP-H2B were subjected to the same time-lapse imaging experiments. These experiments clearly indicated the Lck-Cherry exhibited a very similar increase in cortical signals during polar body emission (Figure 2B, 00:00–00:10). The similarity between the two probes was more evident in *xz*-plane view (Figure 2C), which indicated membrane thickening around the base of the polar body, in contrast to the increase of brightness of Lck-GCaMP3 signal after pricking (Figure 1B). Colocalization of the two probes was further confirmed in oocytes injected with the two fluorescence probes imaged during first-polar-body emission (Figure 2D). One obvious difference was the presence of Lck-GCaMP3 signal at the spindle pole (arrow in Figure 2, A and D) and the corresponding lack of Lck-Cherry signal (Figure 2, B and D).

Similar Lck-GCaMP3 signal was observed during second-polar-body emission (Figure 2E). In this case, both the initial calcium wave (Figure 2E, 00:03–00:06) and later accumulation at the base the polar body (00:20–00:22) were observed. Anaphase II was noted at 00:12 in this oocyte. Of interest, the (metaphase II) spindle pole signal was initially very weak (Figure 2E, 00:00, arrow) but became brighter (00:02) slightly ahead of the neighboring cortical region (00:03). The spindle pole signal remained stronger as the calcium wave subsided (00:06–00:09). These results suggest that the spindle pole signals exhibited by Lck-GCaMP3 in meiosis I (Figure 2, A and D) and in metaphase II before egg activation (Figure 2E, 00:00) likely represent enrichment of the fluorescence probe due to a combination of Lck sequence (membrane targeting) and the calcium sensor calmodulin (spindle targeting, see later discussion).

To further determine possible calcium transients in the spindle area, we carried out similar imaging experiments with GCaMP3, the same permutated GFP core, but without the membrane-targeting Lck sequence (Tian *et al.*, 2009). During oocyte maturation, GCaMP3 was slightly enriched at the spindle (Figure 3A, 00:00–00:08) and remained so through anaphase I (Figure 3A, 00:11). Similar enrichment was also observed at metaphase II (Figure 3B, 00:00). However, after pricking (egg activation), GCaMP3 signal increased dramatically in the cortical area and especially at the spindle (Figure 3B, 00:02) and subsided quickly (Figure 3B, 00:03) in a time course similar to that seen with Lck-GCaMP3 (Figure 1B). These data suggest that signals seen at the spindle (GCaMP3) or spindle pole (Lck-GCaMP3) before egg activation likely represent enrichment of the probe. At egg activation, these probes sense the calcium wave (Busa and Nuccitelli, 1985), producing robust fluorescence. Therefore, before egg activation, overall calcium concentrations at the spindle are not significantly higher than in the surrounding area.

Taken together, these data (Figures 1–3) indicated that, unlike egg activation, which features prominent global calcium transients, *Xenopus* oocyte maturation does not involve global calcium transients or overall calcium elevation at the spindle. Furthermore, these data suggest that the apparent accumulation of Lck-GCaMP3 and Lck-Cherry around the site of polar body emission was likely due to new membrane addition.

BAPTA, but not ethylene glycol tetraacetic acid, caused rapid depolymerization of spindle microtubules

Previous studies (Sun and Machaca, 2004; Sun *et al.*, 2008) demonstrated that interfering with intracellular calcium signaling does not inhibit GVBD, but the oocytes do not form polar bodies and exhibit abnormal spindles. To determine the immediate effect of disrupting calcium signaling, we carried out live-cell imaging coupled with timed injection of dibromo (DB)-BAPTA (K_d = 1.6 μM), a calcium buffer previously shown to be effective in inhibiting cleavage in *Xenopus* embryos (Miller *et al.*, 1993). Oocytes injected with fluorescent probes for microtubules and chromosomes were treated with progesterone and monitored by time-lapse confocal imaging. At prometaphase, when the meiosis I spindle is anchored to the oocyte cortex with one pole (Figure 4A; DBB alone, 00:00), DB-BAPTA was injected. Within a few minutes of DB-BAPTA injection, corresponding to the time for the chelator to diffuse from the injection site to the animal pole where the spindle resides (Miller *et al.*, 1993), the bulk of spindle microtubules started to disappear, accompanied by the clustering of chromosomes to the cortex (Figure 4A, DBB alone, 00:04–00:08). Chromosomes remained at the cortex for hours with no sign of polar body emission or oocyte degeneration (unpublished data), indicating metaphase arrest (14 of 14 in five experiments). In contrast, oocytes injected with water were not perturbed and, at ~2 h after GVBD, initiated anaphase (unpublished data) and progressed to emit the first polar body and arrested at metaphase II (10 of 10 in four experiments), as we showed previously (Zhang *et al.*, 2008; Shao *et al.*, 2013).

To test the calcium specificity of DB-BAPTA, we carried out a series of similar buffer injection experiments, except that DB-BAPTA solution was mixed with $CaCl_2$ in ratios of 20:1, 5:1, and 1:1, giving free Ca^{2+} concentrations in the buffer of 0.08, 0.4, and 1.6 μM, respectively (Kline, 1988). Injection of DB-BAPTA buffer with a 20:1 ratio caused rapid spindle collapse, indistinguishable from that with DB-BAPTA alone (unpublished data). DB-BAPTA buffer at a 5:1 ratio caused similar but more gradual spindle collapse (Figure 4A, middle, representative of 19 oocytes in four experiments). DB-BAPTA buffer with a 1:1 ratio did not collapse the spindle in the same time frame (Figure 4A, bottom, representative of 11 oocytes in two experiments). Instead, it caused cortical contraction, similar to egg activation (see *Materials and Methods*). These data clearly indicate that the immediate spindle collapse caused by DB-BAPTA is due to its calcium-buffering action.

To further demonstrate the effect of calcium buffering on spindles, we used an ultraviolet (UV)-labile caged calcium chelator, diazo-2, a caged BAPTA with a low affinity (2.2 μM) that becomes a high-affinity calcium chelator (BAPTA; ~0.1 μM) after photoactivation (Mulligan and Ashley, 1989). Trial experiments indicated that whereas high concentrations of diazo-2 caused microtubule depolymerization similarly to DB-BAPTA, intracellular concentrations less than ~1 mM had no effect on spindle stability or polar body emission (Figure 4B, top, representative of 24 oocytes in three experiments). Therefore we injected 30 nl of 10 mM diazo-2 (or 0.9 mM final intracellular concentration) at prometaphase. The oocytes were incubated for 5–10 min to allow diazo-2 to equilibrate throughout the oocyte before confocal imaging (Figure 4B, bottom, 00:00). Immediately thereafter, the oocyte was subjected to UV excitation through the same microscope lens for 3 min (00:00–00:03). Simultaneous confocal imaging indicated rapid depolymerization of spindle

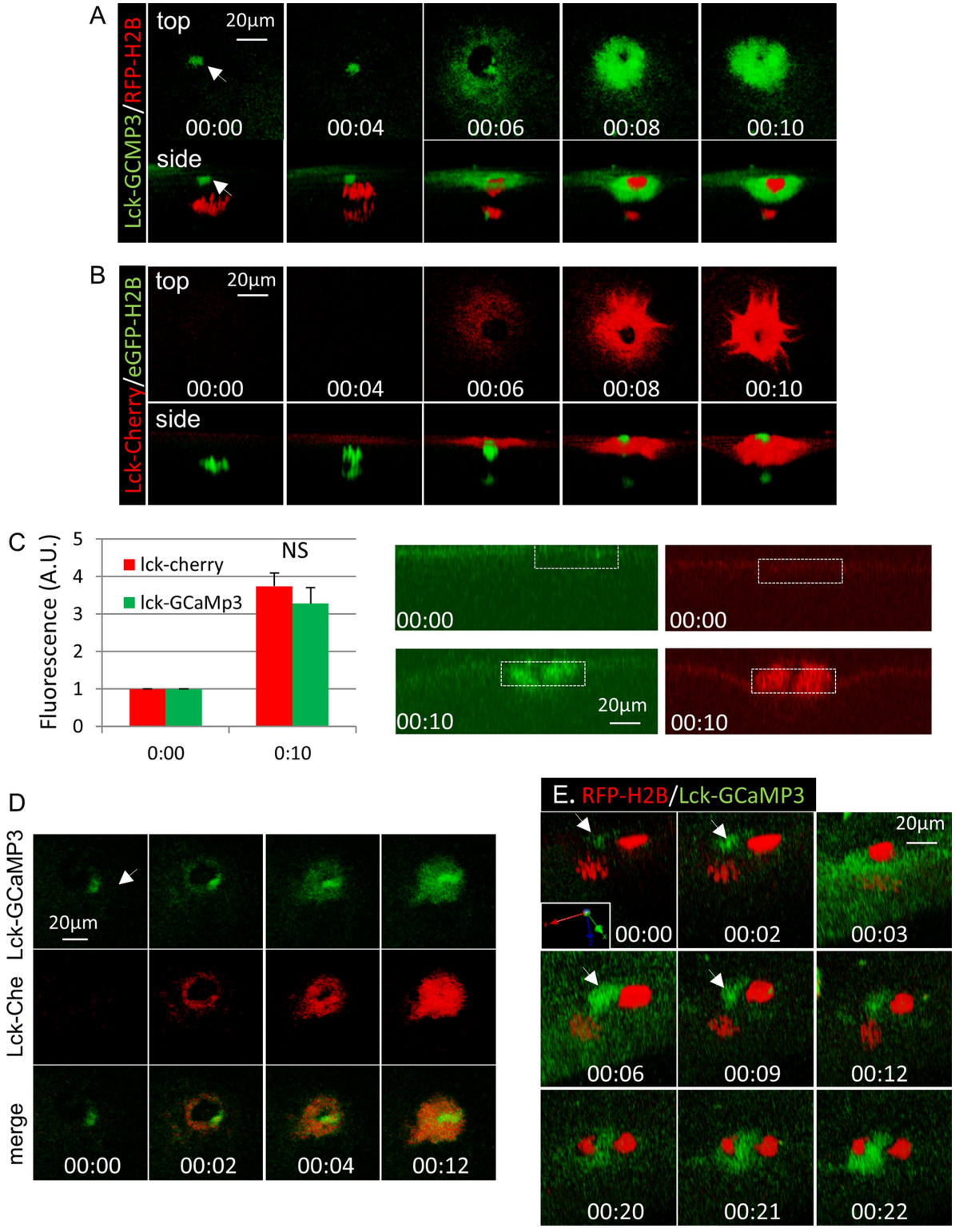

FIGURE 2: Polar body emission involves significant membrane addition. (A) Time series of an oocyte injected with mRNAs for Lck-GCaMP3 and RFE-H2B during first-polar-body emission. Arrow depicts the cortical spindle pole. (B) Time series of an oocyte injected with mRNAs for Lck-mCherry and GFP-H2B during first-polar-body emission. (C) The graph summarizes relative fluorescence at the cortical region around the spindle (white dotted box) at 00:00 and 00:10 of the same oocyte as in B, with values at 00:00 set as 1. Three oocytes, two experiments. NS, not significant. (D) Time series of an oocyte coexpressing Lck-GCaMP3 and Lck-Cherry imaged at similar time points as in A and B. Arrow, cortical spindle pole. (E) Time series (slightly tilted side view, with coordinates shown) of an oocyte injected with Lck-GCaMP3 and RFP-H2B imaged at metaphase II (00:00) and the indicated time after pricking. Arrow depicts the position of the cortical pole of the metaphase II spindle. Anaphase was noted at 00:12.

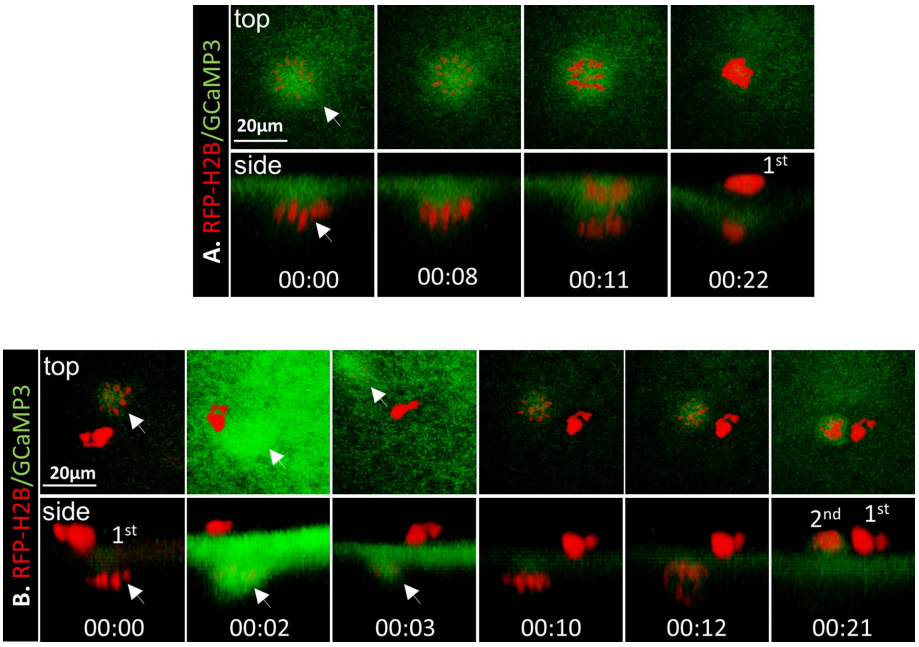

FIGURE 3: GCaMP3 failed to detect spindle-based calcium signals. (A) Time series of an oocyte injected with GCaMP3 and RFP-H2B imaged during first (1st) polar body emission. Arrow depicts metaphase I spindle (00:00 = 115 min after GVBD). Representative of three oocytes. (B) Time series of an oocyte injected with GCaMP3 and RFP-H2B imaged at metaphase II (00:00) and the indicated time after pricking. Arrow depicts metaphase II spindle. 2nd, second polar body. Representative of six oocytes.

microtubules and chromosome clustering (00:02–00:06), similarly to oocytes injected with DB-BAPTA alone (Figure 4A, top). UV excitation of oocytes not injected with diazo-2 did not affect spindle morphology or polar body emission (unpublished data), as we reported previously (Shao *et al.*, 2013).

The foregoing results—rapid depolymerization of spindle microtubules in the presence of BAPTA-based calcium buffers and yet no evidence of overall increase of calcium at the spindle compared with the surrounding cytoplasm—suggest the involvement of highly localized, or nanodomain, calcium signaling (Neher, 1998; Wang and Augustine, 2014). In a calcium nanodomain, the calcium channel and the calcium sensor are within tens of nanometers, often in the same molecular complex. High concentrations of calcium released at the mouth of the channel binds rapidly (microsecond scale) to the calcium sensor, producing a biological response, before falling rapidly. The nanodomain calcium is so transient both spatially and temporally that it is not amenable to conventional microscopy using mobile calcium indicators (Tay *et al.*, 2012). Nanodmain calcium signaling is effectively buffered by the fast calcium buffer BAPTA and its derivatives but not to ethylene glycol tetraacetic acid (EGTA; Adler *et al.*, 1991), which is a slow calcium buffer at physiological pH (Tsien, 1980). To test this possibility, we carried out similar injection experiments with EGTA. Indeed, EGTA injection (30 nl of 25 mM per oocyte) at prometaphase caused no noticeable change in spindle structure, nor did it inhibit first-polar-body emission (Figure 4C, representative of 38 oocytes in five experiments). Injecting 60 nl of 25 mM EGTA (4.5 mM intracellular concentration) or mixing EGTA with various concentrations of calcium (5:1 and 1:1) before buffer injection produced identical results (unpublished data).

To ascertain that both EGTA and DB-BAPTA function properly to buffer calcium in *Xenopus* oocytes, we determined the effect of DB-BAPTA and EGTA on egg activation, which requires global calcium elevation (Figure 1B). Oocytes were injected with chromosome and microtubule probes and treated overnight with progesterone. Mature (metaphase II) eggs were injected with water (Figure 5A, 00:00), immediately followed by time-lapse imaging. The injection served to activate the egg (pricking), as evidenced by cortical contraction, anaphase II (00:12–00:14), and emission of the second polar body (00:31). Injection of DB-BAPTA to metaphase II eggs (Figure 5B, 00:00) did not cause cortical contraction, indicating that DB-BAPTA inhibited egg activation. However, metaphase II spindle collapsed rapidly, accompanied by chromosome clustering (Figure 5B, 00:02–00:15), similarly to prometaphase oocytes injected with DB-BAPTA (Figure 4A, top). EGTA similarly inhibited egg activation (no cortical contraction) but, in contrast to DB-BAPTA, did not cause spindle collapse at all (Figure 5C, 00:00–00:32). As summarized in Table 1, with the exception of DB-BAPTA-1:1, all buffers inhibited egg activation. DB-BAPTA buffered with equal molar ratio of Ca^{2+} has a free Ca^{2+} concentration of 1.6 μM, similar to the amplitude of calcium wave (1.2 μM) at fertilization previously determined by others (Busa and Nuccitelli, 1985). Similarly buffered EGTA has 123 nM free Ca^{2+} and thus is capable of inhibiting egg activation (Table 1). These results confirmed that whereas both DB-BAPTA and EGTA effectively buffered the global calcium transients at egg activation, only DB-BAPTA (and diazo-2 after uncaging) was able to buffer the calcium transients required for spindle function.

Differential effects of DB-BAPTA on Cdc42 and RhoA GTPases

To demonstrate further the effect of calcium buffering at later steps of polar body emission, we injected DB-BAPTA at the beginning of anaphase. Specifically, we sought to determine the effect of calcium buffering on Cdc42-mediated membrane protrusion and the simultaneous RhoA contractile ring function (Zhang *et al.*, 2008). In control oocytes, a small amount of eGFP-wGBD was seen at the spindle (Figure 6A, Ctrl, 00:00), as previously reported (Zhang *et al.*, 2008). Soon after anaphase (00:04), a bright eGFP-wGBD "cap" was seen overlaying the protruding polar body chromosomes (00:10, arrow; note the outline of oocyte surface in faint green) and enveloping the polar body (00:16, arrow). Injection of DB-BAPTA at the beginning of anaphase (Figure 6A, DB-BAPTA, 00:04) eliminated eGFP-wGBD signal and prevented membrane protrusion, trapping all chromosomes inside the eggs (00:08–00:22; eight of eight in two experiments). Whereas control oocytes emitted the first polar body (PB) and arrested with a metaphase II spindle similarly anchored to the cortex (Figure 6A, Ctrl, 01:23), DB-BAPTA–injected oocytes failed to emit a polar body, with condensed chromosomes close to the cortex (Figure 6A, DB-BAPTA, 01:50). Therefore DB-BAPTA inhibited Cdc42 activation and prevented membrane protrusion.

Of interest, and in contrast to complete inhibition of Cdc42 activation, DB-BAPTA did not inhibit RhoA activation or inhibit formation of a contractile ring (Figure 6B). Instead, whereas the contractile ring constricted "below," and hence extricated, polar body chromosomes (Figure 6B, Ctrl, 00:11–00:16) in control oocytes, the contractile ring in DB-BAPTA–injected oocytes constricted, futilely, "above" all chromosomes (Figure 6B, DB-BAPTA, 00:08–00:12). The effect of

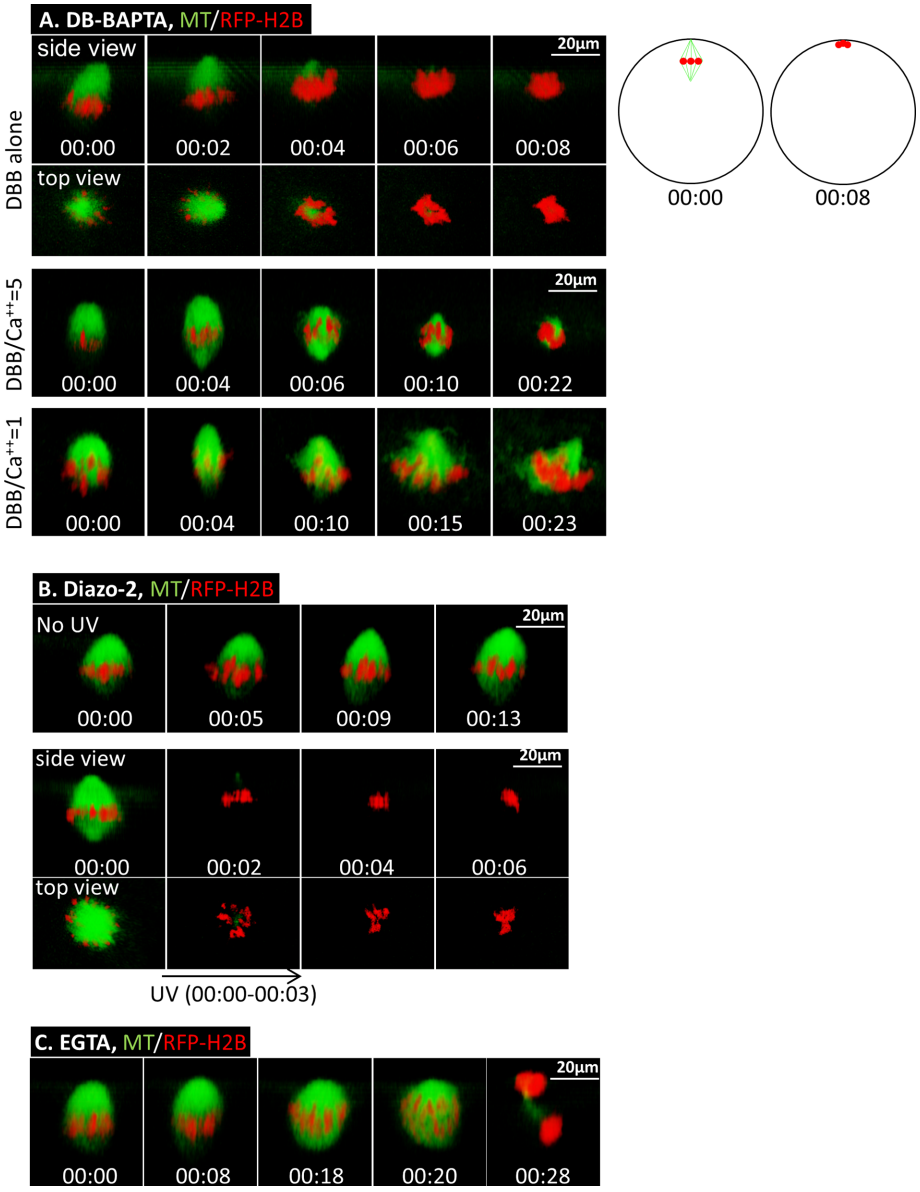

FIGURE 4: BAPTA Ca^{2+} chelators, but not EGTA, cause spindle microtubule depolymerization in meiosis I. (A) Top, time series of an oocyte injected with 30 nl of 25 mM DB-BAPTA at 90 min after GVBD. The oocyte was subjected to time-lapse imaging immediately after DB-BAPTA injection (00:00). The schematics on the right depict side views of oocytes at 0 and 8 min after DB-BAPTA injection, respectively. Middle, time series (side view) of an oocyte injected (60 min after GVBD; 00:00) with 30 nl of 25 mM DB-BAPTA mixed with 5 mM $CaCl_2$, depicting more gradual spindle collapse and chromosome clustering. Bottom, time series (side view) of an oocyte injected with 30 nl of 25 mM DB-BAPTA mixed with 25 mM $CaCl_2$ 60 min after GVBD, depicting no spindle collapse within a similar time frame. This series is composed of four image segments of the same oocyte, necessitated due to the cortical contraction. (B) Top, time series (side view) of an oocyte injected with 30 nl of 10 mM diazo-2 at 90 min after GVBD (00:00) followed by time-lapse imaging. Bottom, time series of an oocyte injected with 30 nl of 10 mM diazo-2 at 90 min after GVBD. Five minutes after diazo-2 injection, the oocyte was imaged (00:00), followed immediately by UV illumination for 3 min (00:00–00:03) and simultaneous time-lapse imaging. (C) Time series (side view) of an oocyte injected with 30 nl of 25 mM of EGTA at 90 min after GVBD. The oocyte was subjected to time-lapse imaging immediately after EGTA injection (00:00) and shows normal anaphase (00:20) and first-polar-body emission (00:28).

DB-BAPTA injection on RhoA contractile ring is reminiscent of the phenotype caused by a dominant-negative Cdc42 mutant (Cdc42N17; Zhang *et al.*, 2008).

Calmodulin is intimately associated with meiosis spindles

The foregoing results, particularly the different sensitivity of spindle integrity to BAPTA and EGTA, strongly suggest that polar body emission in *Xenopus* oocytes requires nanodomain calcium signaling. Nanodomain calcium signaling is not sensitive to EGTA because of the close proximity—within tenths of a nanometer—of the calcium source and calcium sensor, and binding of calcium to the sensor is much more rapid than binding of calcium to EGTA (Neher, 1998; Augustine *et al.*, 2003). One possible calcium senor is the calcium-binding messenger protein calmodulin. *Xenopus* oocytes contain extremely high concentration, 44–59 μM, of calmodulin (Cartaud *et al.*, 1980). Furthermore, calmodulin has been shown in association with the spindle in meiosis I pig oocytes (Fan *et al.*, 2003), meiosis II mouse oocytes (Johnson *et al.*, 1998), and somatic cells (Li *et al.*, 1999).

Oocytes were fixed at the various stages during polar body emission and costained with antibodies against calmodulin and β-tubulin and counterstained with 4′,6-diamidino-2-phenylindole (DAPI). Calmodulin was enriched at the spindle, starting at early (E) prometaphase, when short microtubules emanating from the single patch-shaped microtubule-organizing center capture cortical chromosomes (Gard, 1992; Shao *et al.*, 2012), and throughout prometaphase, metaphase I, anaphase I, and metaphase II, with patterns very similar to those of anti–β-tubulin staining (Figure 7; colocalization coefficients, at any stage, of >0.8). Of interest, the microtubule remnant present within the first polar body was not associated with calmodulin (Figure 7, far right, arrow), suggesting calmodulin's role in functional (spindle) microtubules. We could not consistently inhibit polar body emission using W7 (Su and Eppig, 2002) either added to the medium or by injection (up to 50 μM final intracellular concentration), calmodulin-binding domain peptide 290–309 of CMKII (Ichida *et al.*, 2000; 10–100 nl of 0.5 mM stock solution, per oocyte), or morpholino oligos antisense to *Xenopus* calmodulin (unpublished data). However, the same inhibitors also did not block egg activation (unpublished data). Thus further work with more efficient inhibitor/strategy will be required to establish the functional role of calmodulin in polar body emission.

DISCUSSION

In this study, we combined live-cell imaging with temporally precise application of calcium chelators: timed injection of DB-BAPTA or

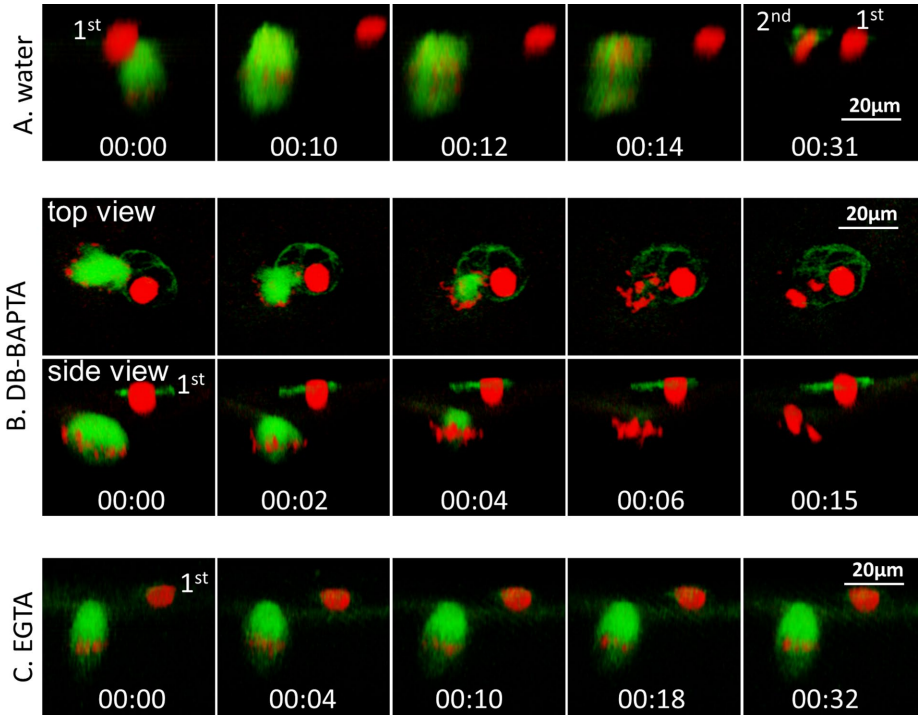

FIGURE 5: Both DB-BAPTA and EGTA buffers inhibited egg activation, but only DB-BAPTA caused collapse of metaphase II spindle. (A) Time series (side view) of a mature egg injected with 30 nl of water, followed immediately by time-lapse imaging (00:00), depicting anaphase (00:12) and emission of the second polar body (00:31). This series is composed of three image segments of the same oocyte, necessitated because significant cortical contraction required repositioning of the oocyte. (B) Time series of a mature egg injected with 30 nl of 25 mM DB-BAPTA (00:00), followed by immediate time-lapse imaging, depicting the lack of egg activation (no cortical contraction) but rapid collapse of metaphase II spindle. (C) Time series (side view) of a mature egg injected with 30 nl of 25 mM EGTA (00:00), followed by immediate time-lapse imaging, depicting no cortical contraction or changes of metaphase II spindle.

EGTA, and UV-induced activation of caged calcium chelator diazo-2 (Mulligan and Ashley, 1989). Our approach has the distinct advantage of revealing the direct effect of intracellular calcium buffering. Our data clearly indicate that BAPTA-based calcium chelators (DB-BAPTA and uncaged diazo-2), but not EGTA, caused rapid collapse of meiosis spindles. The effect of DB-BAPTA was clearly due to calcium buffering, as indicated by the inverse relationship between concentration of free calcium in the buffer and speed of spindle collapse (Figure 4A). DB-BAPTA alone caused immediate collapse of the spindle and clustering of chromosomes to the cortex, subject to diffusion of the buffer from the injection site to the spindle location (Miller *et al.*, 1993). DB-BAPTA/Ca^{2+} mixture in a ratio of 5 (free Ca^{2+} = 400 nM) caused much more gradual spindle collapse and chromosomes clustering. The buffer mixture with a DB-BAPTA/Ca^{2+} ratio of 1 (free Ca^{2+} = 1.6 μM) did not collapse the spindle in the same time frame. Instead, it caused cortical contraction, mimicking the fertilization calcium wave of 1.2 μM amplitude (Busa and Nuccitelli, 1985). With time, the spindle in these oocytes eventually became smaller (unpublished data), presumably because excess free Ca^{2+} eventually dissipates through a combination of sequestration by endogenous organelles (i.e., endoplasmic reticulum [ER]) and calcium buffers and efflux, allowing DB-BAPTA to buffer the spindle-based calcium transients.

	Buffer: Ca^{2+} ratio	Free Ca^{2+} in buffer	Egg activation
DB-BAPTA (25 mM)	Alone		No (28/28)
	5:1	400 nM	No (12/12)
	1:1	1.6 μM	Yes (9/12)
EGTA (25 mM)	Alone		No (32/32)
	5:1	25 nM	No (8/8)
	1:1	123 nM	No (6/6)
Water			Yes (10/11)

Each egg was injected with 30 nl of water or calcium buffers with the indicated buffer:Ca^{2+} ratio and corresponding free Ca^{2+} in the buffer. Numbers in parentheses indicate the number of injected eggs, showing the indicated phenotype—yes or no egg activation—over the total number of injected eggs.

TABLE 1: Buffer injection and egg activation.

The spindle collapse caused by DB-BAPTA injection or UV activation of diazo-2 exhibited a speed identical to that with nocodazole treatment (Shao *et al.*, 2013), suggesting a similar mechanism: inhibition of microtubule polymerization. Consistent with this interpretation, injection of DB-BAPTA at the junction of metaphase-to-anaphase transition inhibited cortical Cdc42 activation and membrane protrusion (Figure 6A), both of which depend on spindle microtubules (Leblanc *et al.*, 2011) and spindle positioning, with one pole anchored to the cortex (Zhang *et al.*, 2008). In contrast, complete collapse of microtubule spindle caused by DB-BAPTA did not inhibit RhoA activation or formation of the contractile ring (Figure 6B), suggesting that chromosomes and/or closely associated microtubule organizing center (MTOC) in these acentrosomal oocytes (Gard, 1992; Schuh and Ellenberg, 2007; Shao *et al.*, 2012) were sufficient to induce the contractile ring. Of interest, in sea urchin embryos, the two asters (MTOCs), placed far enough from each other, can activate RhoA and support complete cytokinesis without microtubule spindle or chromosomes (von Dassow *et al.*, 2009).

The most interesting discovery is the different sensitivity of spindle integrity to BAPTA and EGTA: rapid and complete microtubule depolymerization in the presence of DB-BAPTA but none at all in the presence of EGTA at equal or higher concentrations. This is despite EGTA having an affinity for calcium (123 nM at physiological pH; Qin *et al.*, 1999) that is at least an order of magnitude greater than that of DB-BAPTA (K_d = 1.6 μM) and despite the ability of EGTA to inhibit egg activation in all buffer compositions (Table 1). This different sensitivity is reminiscent of that found in another calcium-mediated process: neurotransmitter release in the presynaptic nerve terminals of squid giant synapse (Adler *et al.*, 1991). A large body of literature has yielded detailed mechanistic understanding of this system and the different responses to BAPTA and EGTA (Neher, 1998; Wang and Augustine, 2014). The close proximity, and indeed the direct molecular contact, of the calcium source (voltage-gated calcium channels) and calcium sensor (the vesicular protein synaptotagmin)

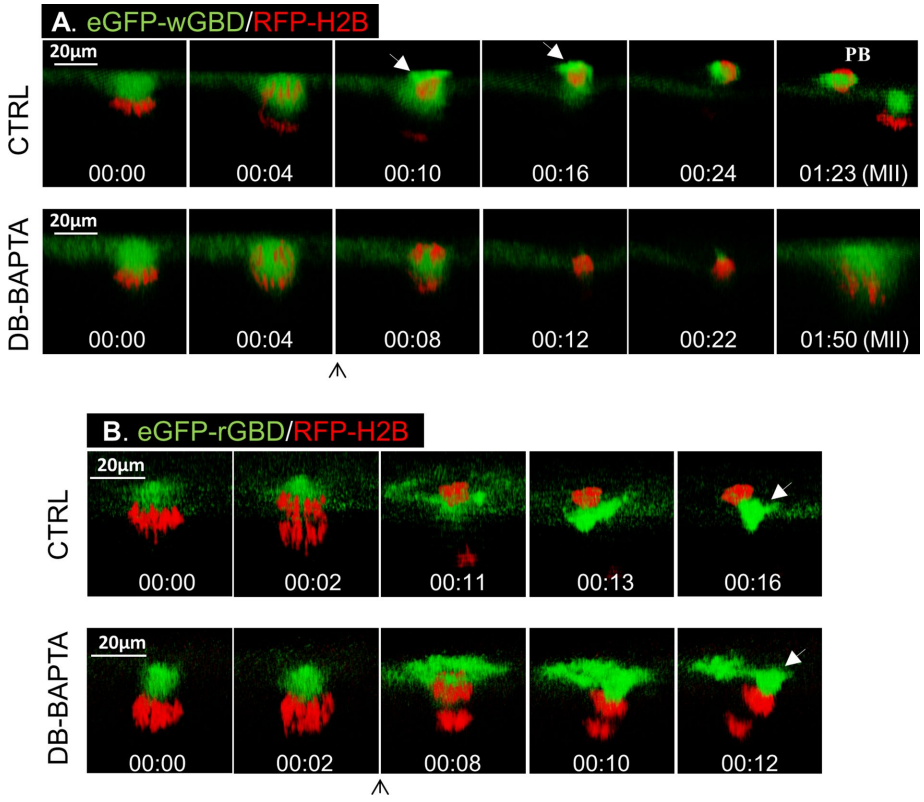

FIGURE 6. DB-BAPTA inhibits Cdc42 activation but not RhoA activation. (A) Top, time series (side view) of a control oocyte showing the active Cdc42 (green) cap overlying the polar body chromosomes (00:10, arrow) and active Cdc42 at the polar body cortex (00:16, arrow). Bottom, time series of an oocyte injected with 20 nl of 30 mM DB-BAPTA immediately after anaphase initiation (upward arrow), depicting the lack of Cdc42 activation or polar body emission. (B) Top, time series (side view) of a control oocyte showing the active RhoA (green) contractile ring (00:11) and constriction "below" the polar body chromosomes (00:13 and 00:16, arrow). Bottom, time series of an oocyte injected with 20 nl of DB-BAPTA immediately after anaphase initiation (upward arrow), showing active RhoA contractile ring (00:08) and constricting "above" both sets of chromosomes (00:12, arrow).

form a calcium signaling unit called a nanodomain (the calcium channel and the sensor are within 20 nm of each other), such that the high local calcium concentration directly, on a time scale of microseconds, drives synaptotagmin-mediated vesicle fusion (exocytosis) and neurotransmitter release. Such calcium signaling is completely insensitive to EGTA, which is a slow Ca^{2+} chelator, because at physiological pH, EGTA is protonated and needs to be completely deprotonated before Ca^{2+} binding can occur (Qin *et al.*, 1999). In fact, it was its pH dependence and slow calcium-binding kinetics that prompted the design and synthesis of BAPTA and the various BAPTA derivatives that are calcium chelators (Tsien, 1980). Whereas BAPTA and its derivatives have the same calcium-binding motifs as EGTA (and hence the same Ca^{2+} selectivity over other divalent cations), BAPTAs are fast calcium chelators with diffusion-limited on-rate and therefore are effective in buffering nanodomain calcium transients (Wang and Augustine, 2014). Our data strongly suggest that spindle formation, more specifically microtubule polymerization, requires spindle-based nanodomain calcium signaling.

The requirement of calcium transients for spindle microtubule polymerization appears to contradict the longstanding view that microtubule polymerization does not require calcium and, in fact, is inhibited by it (Weisenberg, 1972; Olmsted and Borisy, 1975). Of interest, the conclusion of calcium noninvolvement was based on the insensitivity of microtubule polymerization to EGTA. In addition, only very high and nonphysiological concentrations of calcium, 0.5 mM or higher, inhibit microtubule polymerization (Weisenberg, 1972; Olmsted and Borisy, 1975). Physiological calcium concentrations (e.g., 1.2 μM at fertilization; Busa and Nuccitelli, 1985) clearly do not destabilize spindle microtubules or interfere with spindle function. As shown here, pricking (or water injection) caused immediate calcium elevation (Figure 1B), but metaphase II spindle remained stable and completed anaphase and polar body emission (Figure 5A). This is in contrast to BAPTA-type buffers (Figures 4, A and B, and 5B) or nocodazole (Shao *et al.*, 2013), which caused immediate collapse of microtubule spindles and clustering of chromosomes.

The calcium source in the proposed nanodomain calcium signaling is unknown, but it appears not to involve calcium influx. Incubating oocytes in OR2 medium (Ma *et al.*, 2006) without $CaCl_2$ resulted in normal spindle and first polar body (unpublished data). Of interest, numerous studies have reported the association of membrane structures, particularly of nuclear envelop/ER origin, with mitotic apparatus (i.e., microtubules and kinetochores) in both plants and animals (Hepler and Wolniak, 1984), including animal oocytes (Rieder and Nowogrodzki, 1983). Depletion of ER calcium stores using thapsigargin caused spindle defects (Sun and Machaca, 2004), directly implicating the IP3 receptor, since it is the only ER calcium channel in *Xenopus* oocytes (Parys *et al.*, 1992; Kume *et al.*, 1993). It is intriguing that IP3 receptors in *Xenopus* oocytes exhibit submicrometer clusters (~50 nm diameter) containing several tens of channels, with a mean cluster–cluster spacing of ~3 μm (Dargan and Parker, 2003). Intracluster calcium-induced calcium transients are disrupted by BAPTA but minimally affected by EGTA (Dargan and Parker, 2003). However, physiological functions of these IP3 receptor clusters are unknown because the calcium transients are measured under artificial IP3 introduction (Dargan and Parker, 2003).

On the other hand, calmodulin might be a calcium sensor in this proposed calcium-signaling system. First, *Xenopus* oocytes contain an extraordinarily large amount (44–59 μM) of calmodulin (Cartaud *et al.*, 1980). Second, calmodulin is highly enriched at the spindle at all stages of meiosis (Figure 7). Similarly, BAPTA buffers caused immediate microtubule depolymerization at all stages (Figures 4, A and B, and 5B). Given its complete insensitivity to EGTA, the calcium transients required for spindle function must be spindle based (Wang and Augustine, 2014). Third, calmodulin is a common calcium sensor with two calcium-binding domains, each capable of binding two Ca^{2+}. The C-terminal calcium-binding lobe exhibits an on-rate of 350–500 μs, and that of the N-lobe is much slower (20 ms; Malmendal *et al.*, 1999; Park *et al.*, 2008). Calmodulin is also known to bind IP3 receptor and regulates its calcium channel activity (Kasri *et al.*, 2006). It is intriguing that calmodulin has also been implicated in regulating microtubule dynamics via microtubule-associated proteins (Lefevre *et al.*, 2013).

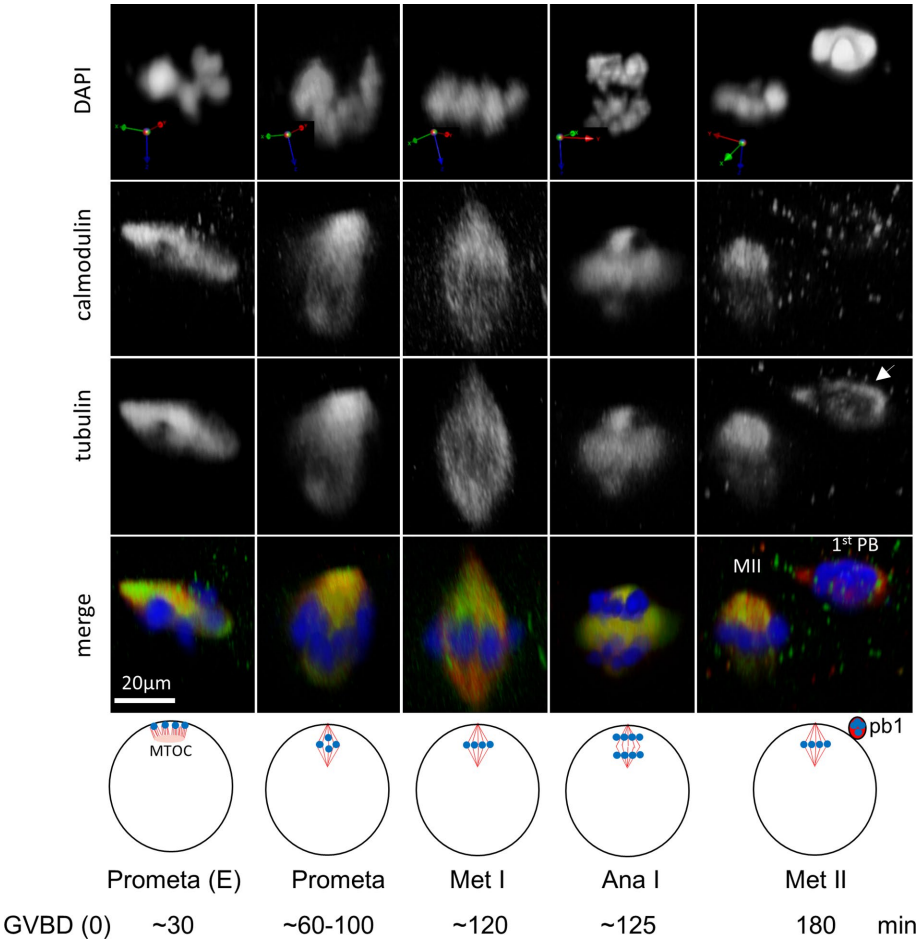

FIGURE 7: Colocalization of calmodulin with spindle microtubules during polar body emission. Typical confocal images of oocytes fixed at the indicated stages, stained with anti-calmodulin and anti-tubulin, and counterstained with DAPI. The projection orientation is indicated for each oocyte, where the *xy*-plane is parallel to the oocyte surface and *z* is perpendicular, pointing toward the center of the oocyte. The approximate time (minutes from GVBD) of each stage is indicated at the bottom. E, early (prometaphase); red, tubulin; green, calmodulin; blue, DNA.

The complete insensitivity of the spindles to high concentrations of EGTA implies that the functional relevant calcium transients are restricted to each nanodomain, dissipating rapidly and within the immediate vicinity of the calcium channels (i.e., IP3 receptors) without functional internanodomain interaction (calcium-induced calcium transients). As such, a global calcium elevation in the spindle area may not be expected, likely explaining the failure of the two calcium probes, GCaMP3 and Lck-GCaMP3, to detect significant calcium signals at the spindle before egg activation. Further imaging work, with far better spatial and temporal resolution, is required to determine the presence of nanodomain calcium signals at the spindle.

MATERIALS AND METHODS

Oocyte collection

Sexually mature *Xenopus laevis* females were obtained from Nasco (Fort Atkinson, WI) and primed with 50 U of pregnant mare gonadotropin 3–10 d before being killed. Oocytes were manually defolliculated (Liu and Liu, 2006) in oocyte culturing medium (OCM) medium (prepared weekly by mixing 480 ml of Leibovitz's L-15 medium, 320 ml of sterile water, 0.32 g of bovine serum albumin, and gentamicin to 0.5 mg/ml, pH 7.6–7.8) and kept at 18°C until use. When stored sparsely with frequent medium changes and cleaning out of dead ones, isolated oocytes can be used for 2–4 d.

Fluorescent probes and other reagents

The following plasmids have been described previously: pCS2-eGFP-H2B (histone 2B), pCS2-mRFP-H2B (Miller and Bement, 2009), pRN3-β5-tubulin-GFP (Verlhac *et al.*, 2000), pCS2-3GFP-EMTB (von Dassow *et al.*, 2009), eGFP-wGBD (for active Cdc42), and eGFP-rGBD (for active RhoA; Benink and Bement, 2005; Zhang *et al.*, 2008). Lck-GCaMP3 and GCaMP3 (Tian *et al.*, 2009; Shigetomi *et al.*, 2010a) were purchased from Addgene and subcloned between *Eco*RI and *Bgl*II sites of pCS2+ vector (Turner and Weintraub, 1994). The DNA sequence encoding the N-terminal 26 amino acids of Lck was amplified by PCR using Lck-GCaMP3 (Shigetomi *et al.*, 2010b) as a template and inserted into pCS2+-C'mCherry vector (von Dassow *et al.*, 2009), generating Lck-Cherry. All cDNA constructs were linearized before in vitro transcription using Ambion SP6 mMESSAGE kit.

Polyclonal anti-calmodulin antibodies (SAB4503194) and monoclonal antibodies against β-tubulin (T5201) were from Sigma-Aldrich (St. Louis, MO).

Oocyte injection, oocyte maturation, and prick activation

All fluorescent probes (mostly mRNAs) were injected at the germinal vesicle stage (GV or intact nucleus) oocytes at least several hours before progesterone treatment to allow protein translation. Oocytes were incubated in OCM plus 1 µM progesterone to trigger oocyte maturation. Oocytes were monitored every 10 min, starting ~2–3 h after the addition of progesterone, for the appearance of a "maturation spot" (Figure 1A) indicative of nuclear envelope breakdown (or GVBD). GVBD oocytes were transferred to fresh OCM without progesterone. DB-BAPTA was dissolved in water and mixed with $CaCl_2$ to the indicated molar ratio according to Kline (1988). EGTA was dissolved in water, adjusted to pH 7 using KOH, and mixed with $CaCl_2$ to the indicated molar ratio. The buffer was injected halfway between the equator and the animal pole (typically 30 nl of 25 mM DB-BAPTA or EGTA per oocyte, or 2.25 mM final intracellular concentration, based on the estimated water-accessible cytoplasm of 333 nl; Snow and Nuccitelli, 1993). To activate mature eggs (arrested at metaphase II), the egg was pricked with a glass needle or injected with water halfway between the animal pole and the equator. Egg activation (Table 1) was assessed by contraction of the pigmented animal hemisphere (cortical contraction; Sive *et al.*, 2000) and confirmed by assessing the presence of second polar body (typically 30 min or longer after egg activation).

Time-lapse confocal laser scanning microscopy

Previously it was demonstrated that anaphase begins ~120 min after GVBD (Ma *et al.*, 2006; Zhang *et al.*, 2008). Accordingly, oocytes were placed in the imaging chamber before anaphase

initiation and imaged for various lengths of time as indicated in figures and/or legends. Imaging was with a 60× oil objective on a Zeiss Axiovert with a Bio-Rad 1024 laser scanning confocal imaging system. Time-lapse imaging is taken at various time intervals (1–3 min) with pixel size of $0.6 \times 0.6 \times 2$ μm (*x*, *y*, and *z*, respectively). Images were three-dimensionally rendered (reconstructed) using Volocity software, with no image deconvolution or any other manipulations. We show three-dimensional (3D) images in "top" view (same direction as the microscope objective), perpendicular "side" view, or *xy*/*xz*/*yz*-plane/slice images (Figures 1B and 2C). All images in a time series were acquired with the same settings during time-lapse imaging of the same oocyte and processed with identical 3D rendering parameters. Time (hh:mm) 00:00 refers to the start of time lapse of each oocyte.

Owing to cortical contraction, especially during the first few minutes after pricking of metaphase II eggs, time-lapse imaging of second-polar-body emission was technically more challenging. Typically, multiple image segments were generated because of the need to reposition the oocytes. Some image distortion might also occur because each of our confocal stacks took up to 20 s to complete.

"Uncaging" of diazo-2

The agent diazo-2 (D-3034; Invitrogen) is a caged, weak calcium chelator (K_d = 2.2 μM), but once photoactivated by UV (~360 nm), it is released as a strong scavenger of calcium (K_d = 73 nM). To "uncage" diazo-2, the oocytes were exposed to UV excitation (Chroma [Bellows Falls, VT] 11000V3, 350/50 nm; 100-W mercury bulb) through a 60× oil objective. The oocyte was simultaneously subjected to confocal imaging through the same objective.

Statistics

All data were analyzed by Student *t* test. $p < 0.05$ was considered statistically significant.

ACKNOWLEDGMENTS

We thank the anonymous reviewers for making constructive comments and suggesting the EGTA experiments. We thank William Bement (University of Wisconsin) for fluorescent probes and Bement and Wayne Chen (University of Calgary, Calgary, Canada) for discussion. Sofia Zhang participated in this project as a summer student intern in 2016. This work was supported by a research grant from the Canadian Institutes of Health Research (MOP 89973) to X.J.L.

REFERENCES

Adler EM, Augustine GJ, Duffy SN, Charlton MP (1991). Alien intracellular calcium chelators attenuate neurotransmitter release at the squid giant synapse. J Neurosci 11, 1496–1507.

Augustine GJ, Santamaria F, Tanaka K (2003). Local calcium signaling in neurons. Neuron 40, 331–346.

Benink HA, Bement WM (2005). Concentric zones of active RhoA and Cdc42 around single cell wounds. J Cell Biol 168, 429–439.

Busa WB, Nuccitelli R (1985). An elevated free cytosolic Ca2+ wave follows fertilization in eggs of the frog, Xenopus laevis. J Cell Biol 100, 1325–1329.

Carroll J, Swann K (1992). Spontaneous cytosolic calcium oscillations driven by inositol trisphosphate occur during in vitro maturation of mouse oocytes. J Biol Chem 267, 11196–11201.

Cartaud A, Ozon R, Walsh MP, Haiech J, Demaille JG (1980). Xenopus laevis oocyte calmodulin in the process of meiotic maturation. J Biol Chem 255, 9404–9408.

Dargan SL, Parker I (2003). Buffer kinetics shape the spatiotemporal patterns of IP3-evoked Ca2+ signals. J Physiol 553, 775–788.

Fan HY, Huo LJ, Meng XQ, Zhong ZS, Hou Y, Chen DY, Sun QY (2003). Involvement of calcium/calmodulin-dependent protein kinase II (CaMKII) in meiotic maturation and activation of pig oocytes. Biol Reprod 69, 1552–1564.

Fontanilla RA, Nuccitelli R (1998). Characterization of the sperm-induced calcium wave in Xenopus eggs using confocal microscopy. Biophys J 75, 2079–2087.

Gard DL (1992). Microtubule organization during maturation of Xenopus oocytes: assembly and rotation of the meiotic spindles. Dev Biol 151, 516–530.

Hepler PK, Wolniak SM (1984). Membranes in the mitotic apparatus: their structure and function. Int Rev Cytol 90, 169–238.

Hyslop LA, Nixon VL, Levasseur M, Chapman F, Chiba K, McDougall A, Venables JP, Elliott DJ, Jones KT (2004). Ca(2+)-promoted cyclin B1 degradation in mouse oocytes requires the establishment of a metaphase arrest. Dev Biol 269, 206–219.

Ichida S, Abe J, Zhang YA, Sugihara K, Imoto K, Wada T, Fujita N, Sohma H (2000). Characteristics of the inhibitory effect of calmodulin on specific [125i]omega-conotoxin GVIA binding to crude membranes from chick brain. Neurochem Res 25, 1629–1635.

Johnson J, Bierle BM, Gallicano GI, Capco DG (1998). Calcium/calmodulin-dependent protein kinase II and calmodulin: regulators of the meiotic spindle in mouse eggs. Dev Biol 204, 464–477.

Kasri NN, Torok K, Galione A, Garnham C, Callewaert G, Missiaen L, Parys JB, De SH (2006). Endogenously bound calmodulin is essential for the function of the inositol 1, 4, 5-trisphosphate receptor. J Biol Chem 281, 8332–8338.

Kline D (1988). Calcium-dependent events at fertilization of the frog egg: injection of a calcium buffer blocks ion channel opening, exocytosis, and formation of pronuclei. Dev Biol 126, 346–361.

Kume S, Muto A, Aruga J, Nakagawa T, Michikawa T, Furuichi T, Nakade S, Okano H, Mikoshiba K (1993). The Xenopus IP3 receptor: structure, function, and localization in oocytes and eggs. Cell 73, 555–570.

Leblanc J, Zhang X, McKee D, Wang ZB, Li R, Ma C, Sun QY, Liu XJ (2011). The small GTPase Cdc42 promotes membrane protrusion during polar body emission via ARP2-nucleated actin polymerization. Mol Hum Reprod 17, 305–316.

Lefevre J, Savarin P, Gans P, Hamon L, Clement MJ, David MO, Bosc C, Andrieux A, Curmi PA (2013). Structural basis for the association of MAP6 protein with microtubules and its regulation by calmodulin. J Biol Chem 288, 24910–24922.

Li CJ, Heim R, Lu P, Pu Y, Tsien RY, Chang DC (1999). Dynamic redistribution of calmodulin in HeLa cells during cell division as revealed by a GFP-calmodulin fusion protein technique. J Cell Sci 112, 1567–1577.

Liu XS, Liu XJ (2006). Oocyte isolation and enucleation. Methods Mol Biol 322, 31–41.

Lorca T, Cruzalegui FH, Fesquet D, Cavadore JC, Mery J, Means A, Doree M (1993). Calmodulin-dependent protein kinase II mediates inactivation of MPF and CSF upon fertilization of Xenopus eggs. Nature 366, 270–273.

Ma C, Benink HA, Cheng D, Montplaisir V, Wang L, Xi Y, Zheng PP, Bement WM, Liu XJ (2006). Cdc42 activation couples spindle positioning to first polar body formation in oocyte maturation. Curr Biol 16, 214–220.

Madgwick S, Levasseur M, Jones KT (2005). Calmodulin-dependent protein kinase II, and not protein kinase C, is sufficient for triggering cell-cycle resumption in mammalian eggs. J Cell Sci 118, 3849–3859.

Malmendal A, Evenas J, Forsen S, Akke M (1999). Structural dynamics in the C-terminal domain of calmodulin at low calcium levels. J Mol Biol 293, 883–899.

Marangos P, Carroll J (2004). Fertilization and InsP3-induced Ca2+ release stimulate a persistent increase in the rate of degradation of cyclin B1 specifically in mature mouse oocytes. Dev Biol 272, 26–38.

Miao YL, Stein P, Jefferson WN, Padilla-Banks E, Williams CJ (2012). Calcium influx-mediated signaling is required for complete mouse egg activation. Proc Natl Acad Sci USA 109, 4169–4174.

Miller AL, Bement WM (2009). Regulation of cytokinesis by Rho GTPase flux. Nat Cell Biol 11, 71–77.

Miller AL, Fluck RA, McLaughlin JA, Jaffe LF (1993). Calcium buffer injections inhibit cytokinesis in Xenopus eggs. J Cell Sci 106, 523–534.

Miyazaki S (2007). Intracellular calcium oscillations in mammalian eggs at fertilization. J Physiol 584, 713–714.

Mulligan IP, Ashley CC (1989). Rapid relaxation of single frog skeletal muscle fibres following laser flash photolysis of the caged calcium chelator, diazo-2. FEBS Lett 255, 196–200.

Nakai J, Ohkura M, Imoto K (2001). A high signal-to-noise Ca(2+) probe composed of a single green fluorescent protein. Nat Biotechnol 19, 137–141.

Neher E (1998). Vesicle pools and Ca2+ microdomains: new tools for understanding their roles in neurotransmitter release. Neuron 20, 389–399.

Olmsted JB, Borisy GG (1975). Ionic and nucleotide requirements for microtubule polymerization in vitro. Biochemistry 14, 2996–3005.
Ozil JP (1998). Role of calcium oscillations in mammalian egg activation: experimental approach. Biophys Chem 72, 141–152.
Park HY, Kim SA, Korlach J, Rhoades E, Kwok LW, Zipfel WR, Waxham MN, Webb WW, Pollack L (2008). Conformational changes of calmodulin upon Ca2+ binding studied with a microfluidic mixer. Proc Natl Acad Sci USA 105, 542–547.
Parys JB, Sernett SW, DeLisle S, Snyder PM, Welsh MJ, Campbell KP (1992). Isolation, characterization, and localization of the inositol 1, 4, 5-trisphosphate receptor protein in Xenopus laevis oocytes. J Biol Chem 267, 18776–18782.
Qin N, Olcese R, Bransby M, Lin T, Birnbaumer L (1999). Ca2+-induced inhibition of the cardiac Ca2 +channel depends on calmodulin. Proc Natl Acad Sci USA 96, 2435–2438.
Rieder CL, Nowogrodzki R (1983). Intranuclear membranes and the formation of the first meiotic spindle in Xenos peckii (Acroschismus wheeleri) oocytes. J Cell Biol 97, 1144–1155.
Schuh M, Ellenberg J (2007). Self-organization of MTOCs replaces centrosome function during acentrosomal spindle assembly in live mouse oocytes. Cell 130, 484–498.
Shao H, Li R, Ma C, Chen E, Liu XJ (2013). Xenopus oocyte meiosis lacks spindle assembly checkpoint control. J Cell Biol 201, 191–200.
Shao H, Ma C, Zhang X, Li R, Miller AL, Bement WM, Liu XJ (2012). Aurora B regulates spindle bipolarity in meiosis in vertebrate oocytes. Cell Cycle 11, 2672–2680.
Shigetomi E, Kracun S, Khakh BS (2010a). Monitoring astrocyte calcium microdomains with improved membrane targeted GCaMP reporters. Neuron Glia Biol 6, 183–191.
Shigetomi E, Kracun S, Sofroniew MV, Khakh BS (2010b). A genetically targeted optical sensor to monitor calcium signals in astrocyte processes. Nat Neurosci 13, 759–766.
Sive HL, Grainger RM, Harland RM (2000). Early Development of Xenopus laevis: A Laboratory Manual, Cold Spring Harbor, NY: Cold Spring Harbor Laboratory Press.
Snow P, Nuccitelli R (1993). Calcium buffer injections delay cleavage in Xenopus laevis blastomeres. J Cell Biol 122, 387–394.
Su YQ, Eppig JJ (2002). Evidence that multifunctional calcium/calmodulin-dependent protein kinase II (CaM KII) participates in the meiotic maturation of mouse oocytes. Mol Reprod Dev 61, 560–569.
Sun L, Hodeify R, Haun S, Charlesworth A, MacNicol AM, Ponnappan S, Ponnappan U, Prigent C, Machaca K (2008). Ca2+ homeostasis regulates Xenopus oocyte maturation. Biol Reprod 78, 726–735.
Sun L, Machaca K (2004). Ca(2+)(cyt) negatively regulates the initiation of oocyte maturation. J Cell Biol 165, 63–75.
Tay LH, Dick IE, Yang W, Mank M, Griesbeck O, Yue DT (2012). Nanodomain Ca(2)(+) of Ca(2)(+) channels detected by a tethered genetically encoded Ca(2)(+) sensor. Nat Commun 3, 778.
Tian L, Hires SA, Mao T, Huber D, Chiappe ME, Chalasani SH, Petreanu L, Akerboom J, McKinney SA, Schreiter ER, *et al*. (2009). Imaging neural activity in worms, flies and mice with improved GCaMP calcium indicators. Nat Methods 6, 875–881.
Tombes RM, Simerly C, Borisy GG, Schatten G (1992). Meiosis, egg activation, and nuclear envelope breakdown are differentially reliant on Ca2+, whereas germinal vesicle breakdown is Ca2+ independent in the mouse oocyte. J Cell Biol 117, 799–811.
Tsien RY (1980). New calcium indicators and buffers with high selectivity against magnesium and protons: design, synthesis, and properties of prototype structures. Biochemistry 19, 2396–2404.
Turner DL, Weintraub H (1994). Expression of *achaete-scute homology 3* in *Xenopus* embryos converts ectodermal cells to a neural fate. Genes Dev 8, 1434–1447.
Verlhac MH, Lefebvre C, Guillaud P, Rassinier P, Maro B (2000). Asymmetric division in mouse oocytes: with or without Mos. Curr Biol 10, 1303–1306.
von Dassow G, Verbrugghe KJ, Miller AL, Sider JR, Bement WM (2009). Action at a distance during cytokinesis. J Cell Biol 187, 831–845.
Wang LY, Augustine GJ (2014). Presynaptic nanodomains: a tale of two synapses. Front Cell Neurosci 8, 455.
Weisenberg RC (1972). Microtubule formation in vitro in solutions containing low calcium concentrations. Science 177, 1104–1105.
Whitaker M (2006). Calcium at fertilization and in early development. Physiol Rev 86, 25–88.
Yurchak LK, Hardwick JS, Amrein K, Pierno K, Sefton BM (1996). Stimulation of phosphorylation of Tyr394 by hydrogen peroxide reactivates biologically inactive, non-membrane-bound forms of Lck. J Biol Chem 271, 12549–12554.
Zhang X, Ma C, Miller AL, Katbi HA, Bement WM, Liu XJ (2008). Polar body emission requires a RhoA contractile ring and Cdc42-mediated membrane protrusion. Dev Cell 15, 386–400.